Effects of entrance channels on the evaporation residue yields in reactions leading to the ^{220}Th compound nucleus

K. Kim* and Y. Kim
Rare Isotope Science Project, Institute for Basic Science, Daejeon 305-811, Korea

A. K. Nasirov†
Joint Institute for Nuclear Research, Joliot-Curie 6, 141980 Dubna, Russia;
Institute of Nuclear Physics, Ulugbek, 100214 Tashkent, Uzbekistan;
and Kyungpook National University, 702-701 Daegu, Korea

G. Mandaglio
Dipartimento di Fisica e di Scienze della Terra dell'Università di Messina, Salita Sperone 31, 98166 Messina, Italy;
Istituto Nazionale di Fisica Nucleare, Sezione di Catania, Italy;
and Centro Siciliano di Fisica Nucleare e Struttura della Materia, 95125 Catania, Italy

G. Giardina
Dipartimento di Fisica e di Scienze della Terra dell'Università di Messina, Salita Sperone 31, 98166 Messina, Italy
and Istituto Nazionale di Fisica Nucleare, Sezione di Catania, Italy

(Received 26 November 2014; revised manuscript received 5 March 2015; published 11 June 2015)

The evaporation residue yields from the compound nuclei ^{220}Th formed in the $^{16}O + ^{204}Pb$, $^{40}Ar + ^{180}Hf$, $^{82}Se + ^{138}Ba$, and $^{124}Sn + ^{96}Zr$ reactions are analyzed to study the entrance channel effects by comparison of the capture, fusion, and evaporation residue cross sections calculated by the combined dinuclear system (DNS) and advanced statistical models. The difference between evaporation residue (ER) cross sections can be related to the stages of compound nucleus formation and/or its survival against fission. The sensitivity of both stages in the evolution of the DNS up to the evaporation residue formation to the angular momentum of DNS is studied. The difference between fusion excitation functions is explained by the hindrance to complete fusion due to the larger intrinsic fusion barrier $B^*_{\rm fus}$ for the transformation of the DNS into a compound nucleus and the increase of the quasifission contribution due to the decreasing of the quasifission barrier $B_{\rm qf}$ as a function of the angular momentum. The largest value of the ER residue yields in the very mass asymmetric $^{16}O + ^{204}Pb$ reaction is related to the large fusion probability and to the relatively low threshold of the excitation energy of the compound nucleus. Due to the large threshold of the excitation energy (35 MeV) of the $^{40}Ar + ^{180}Hf$ reaction, it produces ER yields less than the almost mass symmetric $^{82}Se + ^{138}Ba$ reaction having the lowest threshold value (12 MeV).

DOI: 10.1103/PhysRevC.91.064608 PACS number(s): 25.70.Jj, 25.70.Gh

I. INTRODUCTION

The continuance and complexity of processes preceding the formation of reaction products in heavy ion collisions at low energies are of interest in theoretical and experimental studies [1]. Due to the very transient nature of these processes it is impossible to observe how they occur. Comprehension about the role of the shape and structure of the colliding nuclei in the formation of the observed products can be established by comparison of the experimental data obtained for reactions with different projectile and target nuclei leading to the formation of the same compound nucleus (CN) [2–7]. In all of these works, the results of the comparisons led to the same conclusions: the ER cross sections of the same heated and rotating CN are different even when they are formed at beam energies leading to the same value of the excitation energy $E^*_{\rm CN}$. The main conclusion of the authors in interpretations of the observed differences between ER cross sections is the appearance of hindrance to complete fusion in the stage of CN formation. In the 1980s the extra-extra-push model, the surface friction model, and "dissipative-diabatic-dynamics" model were applied to reproduce the mean values of the barrier of the reaction [2]. In these studies the role of the orbital angular momentum ($L = \ell\hbar$) in the mechanism of the DNS formation and its transformation into the CN were not considered. The rate of the hindrance is determined by the peculiarities of the potential energy surface (PES) [4–8] which contain shell effects of the intrinsic structure of interacting nuclei. The hindrance to complete fusion is related to the increase of the competing quasifission events in the evolution of the DNS formed at capture of the projectile by the target. Theoretical studies of the appearance of the quasifission products showed that their yields and mass distributions are determined by the mass (charge) asymmetry of the entrance channel and peculiarities of the potential energy surface (PES). In Ref. [7], the observed fact that the ER cross section of the $^{124}Sn + ^{92}Zr$ reaction is larger than the one of the more mass asymmetric $^{86}Kr + ^{130}Xe$ reaction was explained with the higher value of

*kyungil@ibs.re.kr
†nasirov@jinr.ru

the PES corresponding to the former reaction than the one of the latter reaction. The strong difference between the excitation functions of the evaporation residues measured in $^{16}O + ^{204}Pb$ and $^{96}Zr + ^{124}Sn$ reactions was explained by the dependence of the capture and fusion cross sections on the orbital angular momentum of collision in Ref. [9].

In this work, we have calculated and compared the capture, fusion, and ER cross sections of the four reactions forming ^{220}Th which have different mass asymmetries: $^{16}O + ^{204}Pb$, $^{40}Ar + ^{180}Hf$, $^{82}Se + ^{138}Ba$, and $^{124}Sn + ^{96}Zr$. The role of the orbital angular momentum in the formation of a compound nucleus is demonstrated.

II. OUTLINE OF THE APPROACH

The study of the main processes taking place in heavy ion collisions near the Coulomb barrier energies is based on calculations of the incoming path of the projectile nucleus and finding the capture probability, taking into account the possibility of interaction with different orientation angles of the axial symmetry axis of a deformed nuclei [10–12]. Also, the surface vibrations of the nuclei, which are spherical in the ground state and have deformed shape in the first excited 2^+ state, are taken into consideration. The final results are averaged over all orientation angles (α_1 and α_2) of the axial symmetry axis of deformed nuclei relative to the beam direction or vibrational states of the spherical nuclei. These procedures are presented in the Appendix A and B sections of this work.

A. Capture of nuclei

Capture of the projectile by the target nucleus is characterized by the full momentum transfer of the relative momentum into the intrinsic degrees of freedom and shape deformation. The capture occurs if the following necessary and sufficient conditions are satisfied. The necessary condition of capture is overcoming the Coulomb barrier by the projectile nucleus to be trapped in the potential well of the PES, which is calculated as a sum of the binding energies of its constituents and the interaction potential energy between them. Figure 1 demonstrates the difference between capture (left panel) and deep inelastic collisions (right panel) as a function of the relative distance $R(t)$ between centers of mass of interacting nuclei for the $^{82}Se + ^{138}Ba$ reaction at $E_{c.m.} = 235$ MeV (left panel) and $E_{c.m.} = 245$ MeV (right panel) with the initial orbital angular momenta $L_0 = 85\hbar$ and $25\hbar$, respectively. The collision dynamics is calculated by the solution of the equation of motions for the relative distance R and angular momentum L. Details of the calculation are presented in Sec. II B.

In Fig. 2, the capture process is shown by the dashed arrow (a) on the PES. But, overcoming the Coulomb barrier by the projectile is not enough for it to be trapped. The condition of sufficiency for capture is the decrease of the relative kinetic energy due to dissipation by friction forces up to values lower than the depth of the potential well [7,10,13]. The potential well is formed due to the competition of the short range nuclear attractive and the Coulomb and centrifugal repulsive potentials. This condition depends on the values of the beam energy and orbital angular momentum, the size of the potential well, and intensity of the friction forces that cause dissipation of the kinetic energy of the relative motions to the internal energy of the two nuclei. So, the trapping of the collision path in the well means that the capture has occurred and the DNS is formed. The lifetime of the DNS is determined by the DNS excitation energy and by the size of the potential well. The height of the inner barrier of the potential well is called the quasifission barrier in our approach. This definition is related

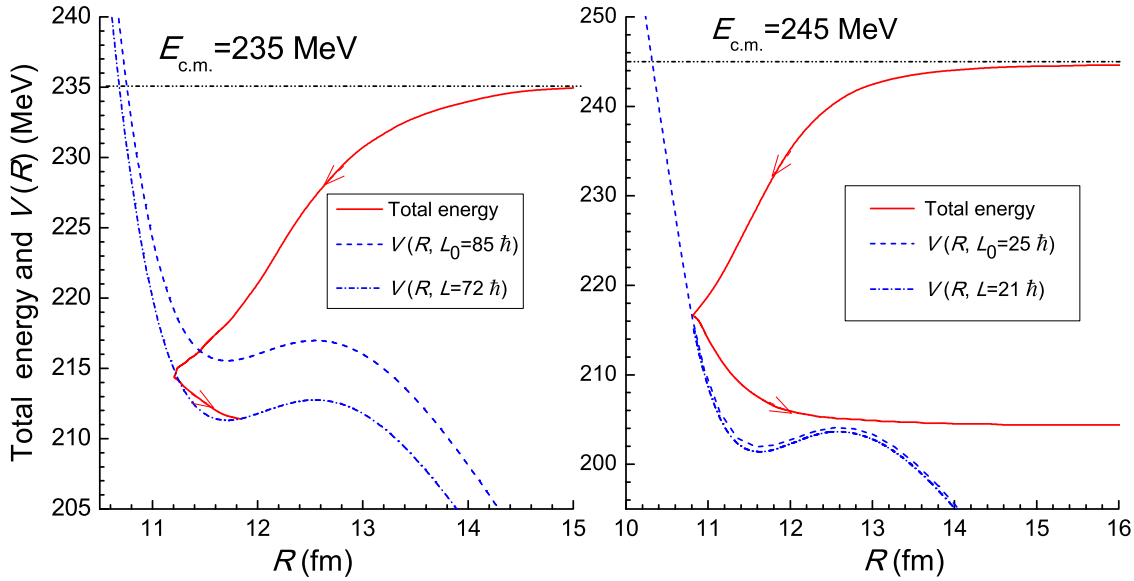

FIG. 1. (Color online) The total energy (solid curve) and nucleus-nucleus potential (dashed and dot-dashed curves) as a function of the relative distance R between centers of mass of colliding nuclei calculated for the $^{82}Se + ^{138}Ba$ reaction at $E_{c.m.} = 235$ MeV (left panel) and $E_{c.m.} = 245$ MeV (right panel) with the initial orbital angular momenta $L_0 = 85\hbar$ and $25\hbar$, respectively. The left panel demonstrates a capture event when the outgoing path of the total energy is trapped in a potential well while the right panel shows a deep inelastic collision with an outgoing path to infinity after dissipation of a sufficient part of the kinetic energy of the relative motion. The dashed and dot-dashed lines are nucleus-nucleus potentials $[V(R)]$ for the ingoing and outgoing paths, calculated for the initial and final values of L.

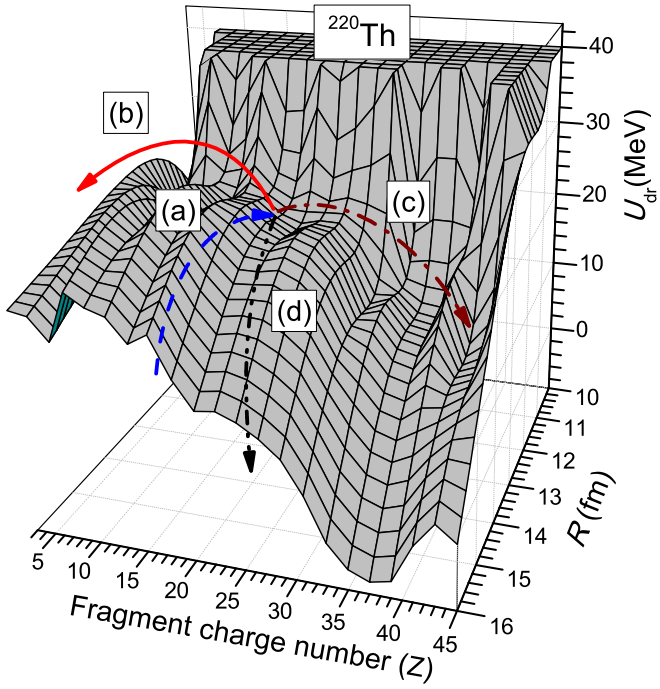

FIG. 2. (Color online) Potential energy surface calculated as a function of the relative distance between the interacting nuclei and charge number (Z) of a fragment for reactions leading to the ^{220}Th CN. Arrow (a) shows the capture path in the entrance channel; arrow (b) shows the direction of the complete fusion by multinucleon transfer from the light nucleus to the heavy one; (c) and (d) arrows show the directions of decay of the DNS into mass symmetric and asymmetric quasifission channels, respectively.

to the quasifission process: the DNS decays without reaching the equilibrated shape of a compound nucleus [10,13,14]. The alternative quasifission process in the evolution of the DNS is complete fusion of its constituent fragments. According to this scenario the capture cross section for a given relative energy in the center-of-mass system and angular momentum value ℓ is the sum of the complete fusion and quasifission cross sections [15]:

$$\sigma_{\rm cap}(E_{\rm c.m.},\ell;\alpha_1,\alpha_2) = \sigma_{\rm fus}(E_{\rm c.m.},\ell;\alpha_1,\alpha_2) + \sigma_{\rm qfis}(E_{\rm c.m.},\ell;\alpha_1,\alpha_2). \quad (1)$$

The capture cross section is determined by the number of partial waves which lead the path of the total energy of colliding nuclei to be trapped in the well of the nucleus-nucleus potential after dissipation of a sufficient part of the initial kinetic energy. The size of the potential well decreases with increasing orbital angular momentum ℓ.

The capture cross section is calculated by the formula

$$\sigma_{\rm capture}(E_{\rm c.m.},\ell;\alpha_1,\alpha_2) = \frac{\lambda^2}{4\pi}\sum_{\ell=0}^{\ell_d}(2\ell+1) \times \mathcal{P}^{\ell}_{\rm capture}(E_{\rm c.m.},\ell;\alpha_1,\alpha_2). \quad (2)$$

Here λ is the de Broglie wavelength of the entrance channel and $\mathcal{P}^{\ell}_{\rm capture}(E_{\rm c.m.},\ell;\alpha_1,\alpha_2)$ is the capture probability which depends on the collision dynamics:

$$\mathcal{P}^{\ell}_{\rm capture}(E_{\rm c.m.},\ell;\alpha_1,\alpha_2) = \begin{cases} 1 & \text{at} \quad \ell_{\rm min} \leqslant \ell \leqslant \ell_d, \\ 0 & \text{if} \quad \ell < \ell_{\rm min} \text{ or } \ell > \ell_d. \end{cases}$$

That means the ℓ values leading to capture can form a "window." It means that the friction coefficient is not so strong as to trap the projectile in the potential well. So, the maximal value of partial waves (ℓ_d) leading to capture is calculated by the solution of the equations of the relative motion of nuclei [5,10]. $\ell_{\rm min}$ is the minimal value of ℓ leading to capture.

B. Potential energy surface

In the framework of the model used in this work, the hindrance to complete fusion is related to the intrinsic fusion barrier $B^*_{\rm fus}$ for the transformation of the DNS into the CN. As a result the DNS decays into two fragments by overcoming the quasifission barrier $B_{\rm qf}$. These quantities are determined by the landscape of the PES, which is calculated for the given values of angular momentum (ℓ) and orientation angles $\{\alpha_i\}$ of the colliding nuclei by the following expression:

$$U(Z_1,A_1,Z_2,A_2,\ell,R,\{\alpha_i\}) = Q_{\rm gg} + V(Z_1,A_1,Z_2,A_2,\ell,\{\alpha_i\};R) - V^{\rm CN}_{\rm rot}(\ell), \quad (3)$$

where $Q_{\rm gg} = B_1 + B_2 - B_{\rm CN}$ is the reaction energy balance; B_1, B_2, and $B_{\rm CN}$ are the binding energies of the interacting nuclei and CN, respectively, which are obtained from the nuclear mass tables in Refs. [16,17].

The nucleus-nucleus potential $V(A,Z,\ell,\{\alpha_i\};R)$ consists of three parts:

$$V(Z_1,A_1,Z_2,A_2,\ell,\{\alpha_i\};R) = V_{\rm Coul}(Z_1,A_1,Z_2,A_2,\{\alpha_i\};R) + V_{\rm nucl}(Z_1,A_1,Z_2,A_2,\{\alpha_i\};R) + V_{\rm rot}(Z_1,A_1,Z_2,A_2,\ell,\{\alpha_i\};R), \quad (4)$$

where $V_{\rm Coul}$, $V_{\rm nucl}$, and $V_{\rm rot}$ are the Coulomb, nuclear, and rotational potentials, respectively. The methods of calculation of these three parts of the nucleus-nucleus potential as a function of the orientation angles of the symmetry axis of the colliding nuclei are presented in Appendix A of Refs. [5,10].

Figure 2 shows the PES calculated at $\ell = 0$ for reactions leading to the ^{220}Th compound nucleus. Arrow (a) shows the capture path in the entrance channel; arrow (b) shows the direction of complete fusion by multinucleon transfer from the light nucleus to the heavy one; (c) and (d) arrows show the directions of decay of the DNS into mass symmetric and asymmetric quasifission channels, respectively. Only some of the paths of the DNS evolution along the solid arrow (b) and surviving against decay along the relative distance lead to complete fusion, i.e., to the CN formation.

In Fig. 3 we illustrate the driving potential $U_{\rm dr}$ which is found by connecting the minima of the potential wells in the sections of PES at all values Z. It is calculated for the ^{82}Se + ^{138}Ba reaction for the spherical shape of ^{138}Ba and the value $\alpha_{\rm Se} = 45^\circ$ of the orientation angle of the

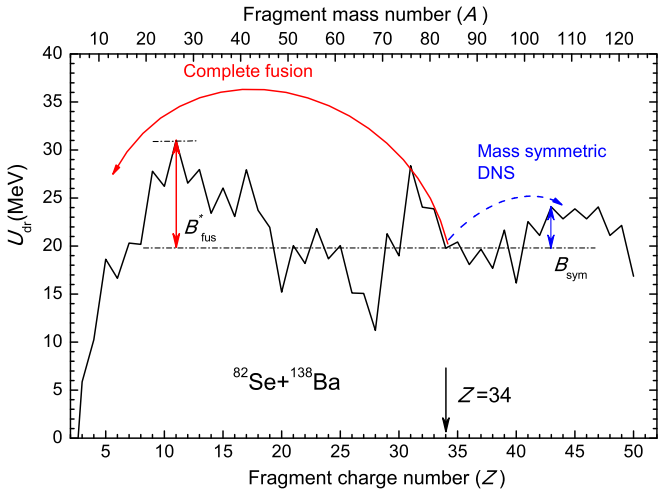

FIG. 3. (Color online) Driving potential of the DNS leading to formation of the ^{220}Th compound nucleus. The barriers B^*_{fus} (B^*_{sym}) pose hindrance to the evolution of the DNS to complete fusion (to reach its symmetric configurations) in the case of the ^{82}Se + ^{138}Ba reaction ($Z = 34$). The curve of the driving potential is obtained for the spherical shape of ^{138}Ba and the value $\alpha_{Se} = 45^\circ$ of the orientation angle of the projectile nucleus relative to the beam direction at $\ell = 0$.

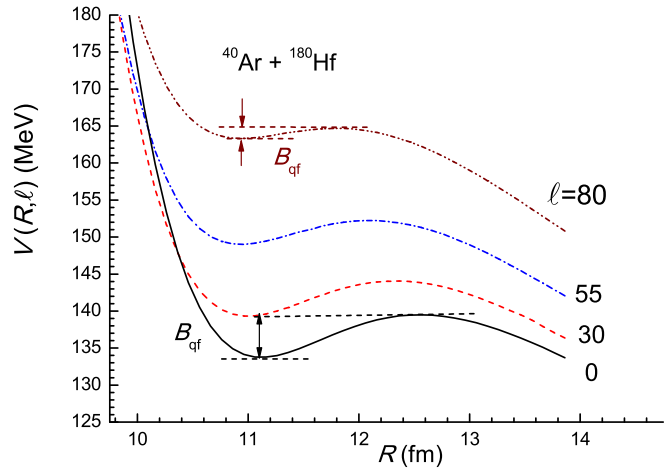

FIG. 4. (Color online) Dependence of the quasifission barrier on the angular momentum of the DNS formed in the ^{40}Ar + ^{180}Hf reaction.

projectile nucleus relative to the beam direction at $\ell = 0$. The hindrance to complete fusion during the evolution of the DNS is determined by the barrier B^*_{fus} which is shown in Fig. 3. It is seen that the height of B^*_{fus} for the more mass symmetric ^{82}Se + ^{138}Ba ($Z = 34$) and ^{124}Sn + ^{96}Zr ($Z = 40$) reactions is larger than the one for the mass asymmetric ^{16}O + ^{204}Pb, ^{40}Ar + ^{180}Hf reactions.

The value of B^*_{fus} depends on the charge and mass asymmetry and shell structure of the DNS fragments (see Fig. 3). Note the shape of the driving potential depends on the orientation angles α_i [10] of the colliding nuclei relative to the beam direction and/or their vibrational states since the nucleus-nucleus interaction potential $V(Z_1, A_1, Z_2, A_2, \ell, \{\alpha_i\}; R)$ is sensitive to α_i [see Eq. (4)]. Consequently, B^*_{fus} depends on the orientation angles or vibrational state of the DNS nuclei. The capture and fusion cross sections are found by averaging over all used values of the orientation angle and/or vibrational states of nuclei by Eqs. (A1) and (B3), respectively. In this work ^{82}Se, ^{96}Zr, and ^{180}Hf are considered to be the deformed nuclei in their ground states (see Table I in Appendix A). The other nuclei have the nearly spherical shape in the ground state and their vibration near spherical shape is taken into account.

The change of the interaction potential due to the increase of the rotational energy by angular momentum calculated for the ^{40}Ar + ^{180}Hf reaction is presented in Fig. 4. It is seen from Fig. 4 that the increase of the angular momentum leads to a decrease of B_{qf}. The quasifission barrier decreases with decreasing DNS charge asymmetry due to the increase of the Coulomb interaction. This dependence of B_{qf} is seen from the landscape of the PES presented in Fig. 2. The stability of the DNS against decay decreases with the decrease of the barrier B_{qf}, and the probability of its transformation into a compound nucleus (complete fusion probability) decreases.

C. Fusion of nuclei

The fusion probability P_{CN} is used to take into account the competition between the complete fusion and decay of the DNS into two fragments (quasifission) to calculate the complete fusion cross section [7,10,18,19]:

$$\sigma_{fus}(E) = \sum_{\ell=0}^{\ell_d(E)} (2\ell + 1)\sigma_{cap}(E,\ell)P_{CN}(E,\ell). \quad (5)$$

The maximum value of ℓ leading to capture $\ell_d(E)$ depends on the beam energy, and it is calculated by the solution of the radial motion equations (see Ref. [10]). Since the capture cross section is equal to the sum of the complete fusion and quasifission cross sections, $\sigma_{cap} = \sigma_{fus} + \sigma_{qfis}$, the quasifission cross section is calculated by the expression

$$\sigma_{qfis}(E) = \sum_{\ell=0}^{\ell_d} (2\ell + 1)\sigma_{cap}(E,\ell)[1 - P_{CN}(E,\ell)]. \quad (6)$$

The competition between fusion and quasifission processes during the DNS evolution is determined by the fusion probability P_{CN} which is calculated by the expression [10]

$$P_{CN}(E^*_{DNS}, \ell; \{\alpha_i\}) = \sum_{Z_{sym}}^{Z_{max}} Y_Z(E^*_{DNS}) P^{(Z)}_{CN}(E^*_{DNS}, \ell; \{\alpha_i\}), \quad (7)$$

where $Z_{sym} = (Z_1 + Z_2)/2$ and Z_{max} corresponds to the point where the driving potential reaches its maximum, i.e., $B^*_{fus}(Z_{max}) = 0$. It is the saddle point on the PES along the Z_1 axis [under arrow (b) in Fig. 2]. The use of Eq. (7) allows us to take into account the fusion probabilities from the DNS charge asymmetry configurations, which differ from the charge numbers of the projectile and target nuclei. The DNS formed at the capture of a projectile by a target is a fluctuating statistical system which rushes to an equilibrium state of the mass and charge distributions by the diffusion process. The DNS lifetime with the given charge asymmetry $Z = Z_1$ and $Z_2 = Z_{CN} - Z$ depends on the depth of the

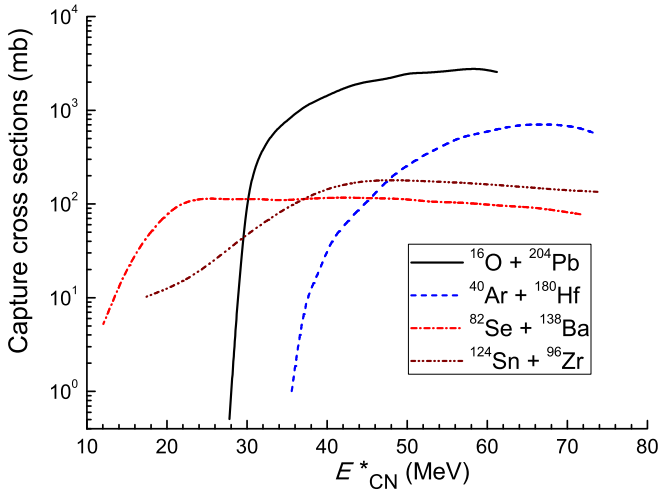

FIG. 5. (Color online) Comparison of the capture excitation functions calculated in this work for the $^{16}O + ^{204}Pb$ (solid line), $^{40}Ar + ^{180}Hf$ (dashed), $^{82}Se + ^{138}Ba$ (dot-dashed), and $^{124}Sn + ^{96}Zr$ (dot-dot-dashed) reactions.

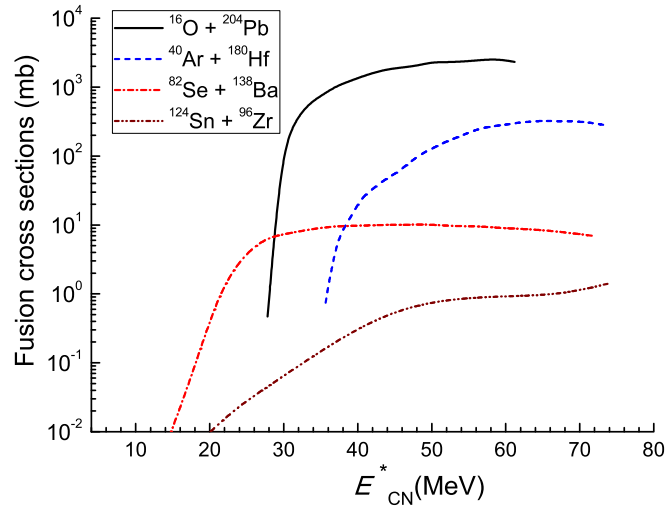

FIG. 6. (Color online) Comparison of the fusion excitation functions calculated in this work for the $^{16}O + ^{204}Pb$ (solid line), $^{40}Ar + ^{180}Hf$ (dashed), $^{82}Se + ^{138}Ba$ (dot-dashed), and $^{124}Sn + ^{96}Zr$ (dot-dot-dashed) reactions.

potential well $B_{qf}^{(Z)}$ and its excitation energy $E_{DNS}^{(Z)*}$. The DNS lifetime may be not enough to reach the equilibrium state with minimal energy in collisions with some values of ℓ and $E_{c.m.}$. It is already known that the barrier B_{fus}^* and B_{qf}, which play crucial roles in complete fusion, depend on the DNS charge asymmetry and angular momentum of the DNS, ℓ. Therefore, we take into account the change of the charge asymmetry by nucleon transfer before the decay of DNS. The mass number A corresponding to the given charge number Z is established by varying A to find its value leading to the minimal value of the PES energy.

III. RESULTS AND DISCUSSION

A. Comparison of capture and fusion cross sections

The influence of peculiarities of the entrance channel on the characteristics of the formed reaction products can be studied by the comparison of experimental data and theoretical results obtained for the reactions leading to the formation of the same CN. The capture and fusion cross sections obtained for the $^{16}O + ^{204}Pb$, $^{40}Ar + ^{180}Hf$, $^{82}Se + ^{138}Ba$, and $^{124}Sn + ^{96}Zr$ reactions are compared in Figs. 5 and 6, respectively.

Hereafter, the CN excitation energy E_{CN}^* is used instead of the collision energy in the center-of-mass system $E_{c.m.}$ for the convenience of comparing reactions having a large difference in the Coulomb barrier energies. The threshold values of E_{CN}^* for the capture excitation functions are determined by the Coulomb barriers of the entrance channel and by the reaction Q_{gg} -value:

$$E_{CN}^*(Z = Z_1) = E_{c.m.}^{(min)}(Z) + Q_{gg}(Z) = V_B^{(Coul)}(Z) + Q_{gg}(Z). \quad (8)$$

Due to large values of $Q_{gg} = -180.516$ MeV and -188.332 MeV for $^{82}Se + ^{138}Ba$ and $^{124}Sn + ^{96}Zr$ reactions, respectively, the entrance channel positions are at the valleys of the PES corresponding to $Z = 34$ and 40. Their positions on the PES are lower than the ones for the $^{16}O + ^{204}Pb$ and $^{40}Ar + ^{180}Hf$ reactions which are placed at $Z = 8$ and 18 (see Fig. 3). So, the difference of the $U(Z,R)$ values as a function of Z appears as a difference in the threshold values of E_{CN}^* at which capture occurs. Due to this reason, connected with the reaction energy balance Q_{gg}, the capture excitation functions of the very mass asymmetric the $^{16}O + ^{204}Pb$ and $^{40}Ar + ^{180}Hf$ reactions are equal to zero at $E_{CN}^* < 28$ MeV and $E_{CN}^* < 35$ MeV, respectively.

The capture excitation functions obtained for the mass asymmetric $^{16}O + ^{204}Pb$ and $^{40}Ar + ^{180}Hf$ reactions are one order of magnitude higher than the ones for the almost symmetric $^{82}Se + ^{138}Ba$ and $^{124}Sn + ^{96}Zr$ reactions at higher excitation energies. This strong difference in the capture cross sections is related to the size of the potential well in the nucleus-nucleus interaction. The increase of beam energy from near the Coulomb barrier energies leads to increase of the number of partial waves contributing to capture and complete fusion.

The Coulomb repulsion is stronger for the almost symmetric reactions in comparison with the one for the asymmetric reactions: $(Z_1Z_2)_{asym} < (Z_1Z_2)_{sym}$. Therefore, strong repulsion forces make the potential well shallower, reducing consequently the maximum number of the partial waves $[\ell_d(E)]$ leading to capture, and the capture cross section decreases [see Eq. (5)].

The excitation functions of complete fusion calculated for the reactions under study are compared in Fig. 6. The fusion excitation function of the almost symmetric reaction is even two orders of magnitude lower than the one of the mass asymmetric reaction.

This fact certifies that the fusion cross section of the charge symmetric reactions is usually smaller than that of the charge asymmetric reactions. As discussed in Sect. II B, the fusion

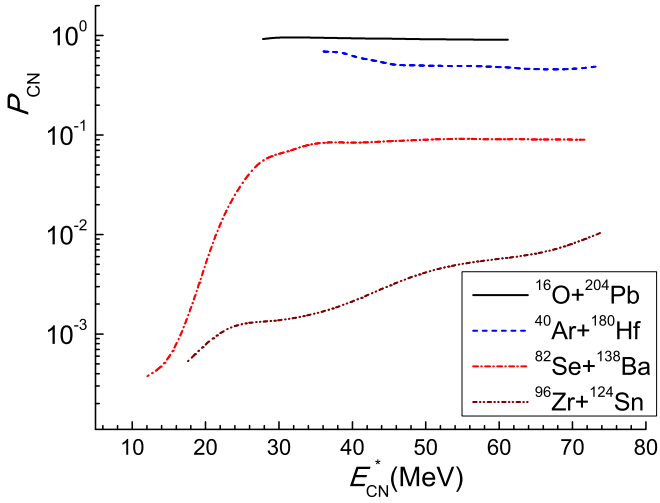

FIG. 7. (Color online) The fusion probability $P_{CN} = \sigma_{fus}/\sigma_{cap}$ calculated for the $^{16}O + ^{204}Pb$, $^{40}Ar + ^{180}Hf$, $^{82}Se + ^{138}Ba$, and $^{124}Sn + ^{96}Zr$ reactions as a function of the CN excitation energy.

probability is sensitive to the intrinsic fusion barrier B^*_{fus} and quasifission barrier B_{qf}.

Figure 7 shows the comparison of the fusion probability P_{CN} as a function of E^*_{CN} for the four above-mentioned reactions leading to the ^{220}Th CN. The behavior of P_{CN} is different for the charge asymmetric and symmetric reactions. As one can see, P_{CN} is about 1 for the $^{16}O + ^{204}Pb$ reaction (very mass asymmetric reaction) on the whole range of excitation energy E^*_{CN}. Therefore, the DNS formed in this reaction evolves almost fully to the CN. In the case of the more symmetric $^{82}Se + ^{138}Ba$ and $^{124}Sn + ^{96}Zr$ reactions the quasifission process is dominant in the evolution of DNS, and the fusion process is strongly hindered.

The strong decrease of P_{CN} at small values of E^*_{CN} for the mass symmetric reactions shows the presence of the large intrinsic fusion barrier, which cannot be overcome by the excited DNS during its evolution and therefore decays through the quasifission channel as shown by the arrows (c) and (d) in Fig. 2.

The analysis of the details in calculations of P_{CN} for the $^{82}Se + ^{138}Ba$ and $^{124}Sn + ^{96}Zr$ reactions shows that the intrinsic fusion barrier B^*_{fus} for the latter reaction is larger than the one for the former reaction for orientation angles of ^{82}Se and ^{96}Zr larger than 30° (see Fig. 3). But at small orientation angles (<30°) of the DNS nuclei, the fusion barriers of the $^{82}Se + ^{138}Ba$ and $^{124}Sn + ^{96}Zr$ reactions are close. Then the increase of B^*_{fus} with the increase of α_{Zr} is faster in the case of the $^{124}Sn + ^{96}Zr$ reaction than the comparable increase in the $^{82}Se + ^{138}Ba$ reaction. B^*_{fus} is not sensitive to α_{Sn} since ^{124}Sn is an almost spherical nucleus and its vibration with amplitude $|\beta_{2^+}| = 0.095$ around the spherical shape is used in the calculation.

Another cause of the difference between fusion barriers of the $^{82}Se + ^{138}Ba$ and $^{124}Sn + ^{96}Zr$ reactions is the difference in their rotational energies, since their moments of inertia are different. Due to this reason the value of the driving potential corresponding to the mass symmetric system $^{124}Sn + ^{96}Zr$ goes down faster than the one of the less symmetric system $^{82}Se + ^{138}Ba$ (for example, see Fig. 3 in Ref. [5]). Therefore, the difference between the values of B^*_{fus} obtained for $^{82}Se + ^{138}Ba$ and $^{124}Sn + ^{96}Zr$ reactions increases with increasing ℓ. The increase of the beam energy leads to increase of the number ℓ contributing to capture while there is a potential well with the barrier $B_{qf} > 0$.

Therefore, the fusion cross section of the $^{124}Sn + ^{96}Zr$ reaction grows more slowly than the one of the $^{82}Se + ^{138}Ba$ reaction. The conclusion is that the behavior of P_{CN} as a function of the excitation energy E^*_{CN} is determined by the dependence of the fusion barrier B^*_{fus} on the orientation angle of the deformed nuclei of the DNS and its angular momentum ℓ.

The small difference between the P_{CN} values obtained for the $^{82}Se + ^{138}Ba$ and $^{124}Sn + ^{96}Zr$ reactions at excitation energy $E^*_{CN} = 20$ MeV is explained by the fact that in the collisions at the beam energies corresponding to this E^*_{CN} only small values of the orientation angles and angular momentum ℓ can contribute to the capture events. As mentioned above, in these conditions, the difference between the values of B^*_{fus} for the $^{82}Se + ^{138}Ba$ and $^{124}Sn + ^{96}Zr$ reactions is small.

We should stress here that the intrinsic fusion barrier B^*_{fus} is nonzero at $\ell = 0$ for the heavy systems which are not very mass asymmetric. This can be seen from Fig. 3 which shows the driving potential of the $^{82}Se + ^{138}Ba$ reaction for the case $\ell = 0$. This means that the quasifission channel, which competes with complete fusion, can take place starting from $\ell = 0$ for such systems [7,10]. The phenomenon of the yield of the quasifission products at small values of ℓ was insinuated by the authors of Ref. [3] by comparing the ER yields and widths of fission mass distributions measured in the $^{30}Si + ^{186}W$ and $^{12}C + ^{204}Pb$ reactions. This conclusion is in contradiction with the well known classification of the reaction channels as a function of the angular momentum. According to that classification, complete fusion always occurs for heavy ion collisions at all values of the angular momentum $\ell < \ell_{cr}$. For a light nuclear system ℓ_{cr} is determined by the properties of the nucleus-nucleus interaction, i.e., by the barrier radius, which is approximately equal to the sum of the radii of the target and projectile nuclei [20]. Our results demonstrate that the above mentioned classification of the reaction channels as function of the angular momentum is not completely correct. The quasifission products can be formed during collisions where $\ell < \ell_{cr}$, and the consideration of them as fusion-fission products leads to the wrong fusion cross sections in the analysis of the experimental data [21].

B. Role of the angular momentum in complete fusion of nuclei

The partial cross sections are important to establish the effect of the entrance channel on the evolution of the DNS formed in reactions with different mass asymmetry of colliding nuclei. It is interesting to compare the angular momentum distributions of the DNS and CN.

The partial capture cross sections calculated for the $^{40}Ar + ^{180}Hf$ and $^{82}Se + ^{138}Ba$ reactions in the ranges of the excitation energy $E^*_{CN} = 32-75$ MeV and $E^*_{CN} = 12-72$ MeV are presented in Figs. 8 and 9, respectively. Comparison of

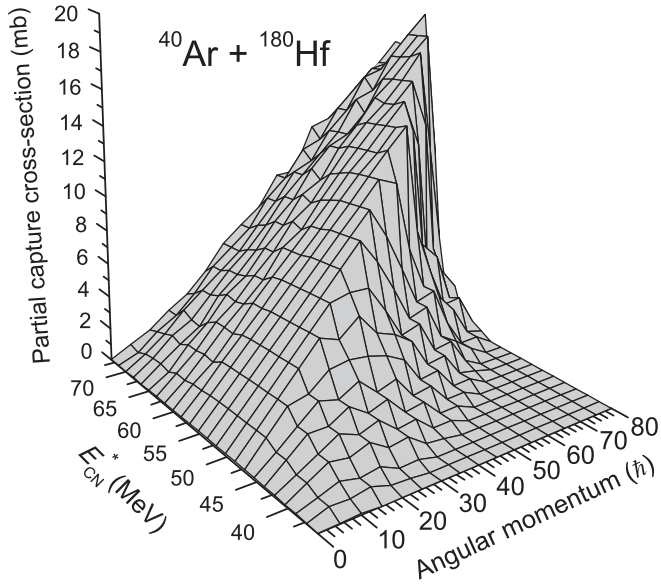

FIG. 8. Partial capture cross section of the ^{40}Ar + ^{180}Hf reaction.

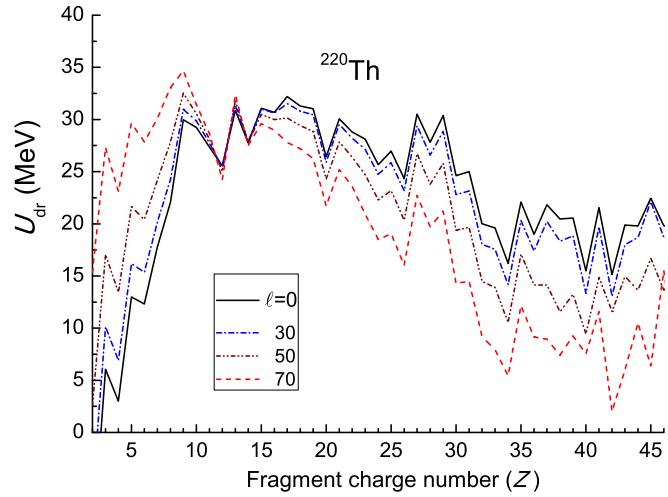

FIG. 10. (Color online) Driving potential for the dinuclear system formed in the ^{82}Se + ^{138}Ba reaction versus the charge number of its fragment for different values of angular momentum ℓ.

these two figures demonstrates the difference in the angular momentum distribution of the DNS formed in these reactions. The small potential well in $V(R)$ for the almost symmetric ^{82}Se + ^{138}Ba reaction causes the smallness of its capture cross section, as presented in Fig. 5.

As already shown in Ref. [19], the CN formed with the same excitation energy in reactions with different mass asymmetry does not have the same partial fusion cross sections, i.e., the angular momentum distribution of the CN will be different. This phenomenon was considered to explain the difference between the experimental values of the excitation functions of the evaporation residue formation in the ^{16}O + ^{204}Pb and ^{96}Zr + ^{124}Sn reactions leading to the same CN ^{220}Th. The first reason is related to the dependence of the height and size of the nucleus-nucleus potential well. The decrease of the size of the potential well leads to the decrease of the capture probability, and, consequently, the fusion probability decreases. Another crucial factor decreasing the fusion probability is an increase of the intrinsic fusion barrier due to the increase of the DNS angular momentum. But, this dependence can be seen from the driving potential calculated for the DNS, which is formed at capture of the projectile by the target. The change of the intrinsic fusion barrier $B^*_{\rm fus}$ as a function of the angular momentum ℓ of the DNS is demonstrated in Fig. 10. As it is manifest from this figure, an increase of the beam energy allows the projectile to be trapped in the potential well with larger values of angular momentum which increase the capture cross section value, but $P_{\rm CN}$ decreases by the increase of $B^*_{\rm fus}$.

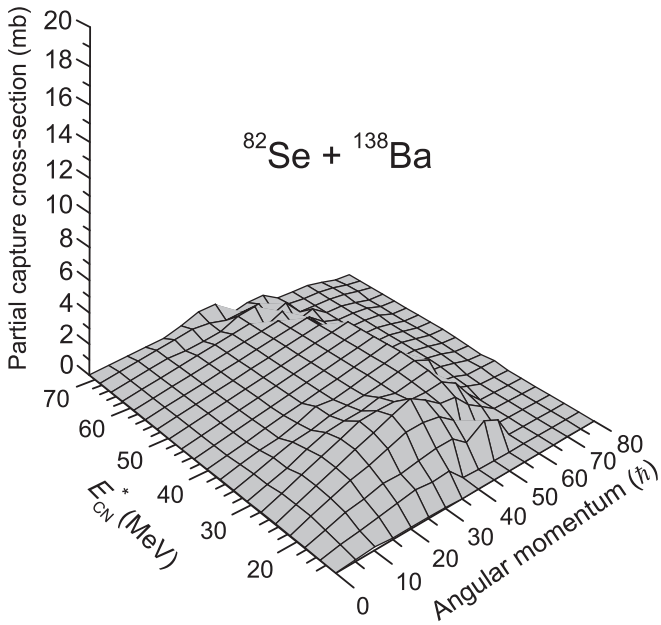

FIG. 9. Partial capture cross section of the ^{82}Se + ^{138}Ba reaction.

The dependence of the quasifission barrier $B_{\rm qf}$ and intrinsic fusion barrier $B^*_{\rm fus}$ on the angular momentum ℓ is presented in Figs. 4 and 10, respectively. The increase of $B^*_{\rm fus}$ decreases the probability of the CN formation. The fusion probability $P_{\rm CN}$ presented in Fig. 7 shows the ratio of the fusion and capture sections averaged over angular momenta for each reaction. It is interesting to know $P_{\rm CN}$ as a function of angular momentum. Figure 11 shows this dependence, which is found from the ratio of the partial fusion and capture cross sections:

$$P_{\rm CN}(E^*_{\rm CN},\ell) = \sigma_{\rm fus}(E^*_{\rm CN},\ell)/\sigma_{\rm cap}(E^*_{\rm CN},\ell). \qquad (9)$$

The partial $P_{\rm CN}(E^*_{\rm CN},\ell)$ values increase with increasing beam energy ($E_{\rm c.m.} = E^*_{\rm CN} - Q_{\rm gg}$) but decrease with the increase of the angular momentum ℓ. The increase of $P_{\rm CN}(E^*_{\rm CN},\ell)$ with increasing $E^*_{\rm CN}$ is clear since the DNS excitation energy increases with increasing $E^*_{\rm CN}$, allowing the DNS to overcome the intrinsic fusion barrier $B^*_{\rm fus}$ more easily. The capture cross section increases due to the factor $(2\ell + 1)$ which should lead to an increase of the fusion cross section, but $P_{\rm CN}$ decreases due to the increase $B^*_{\rm fus}$ as a function of ℓ (see Fig. 10).

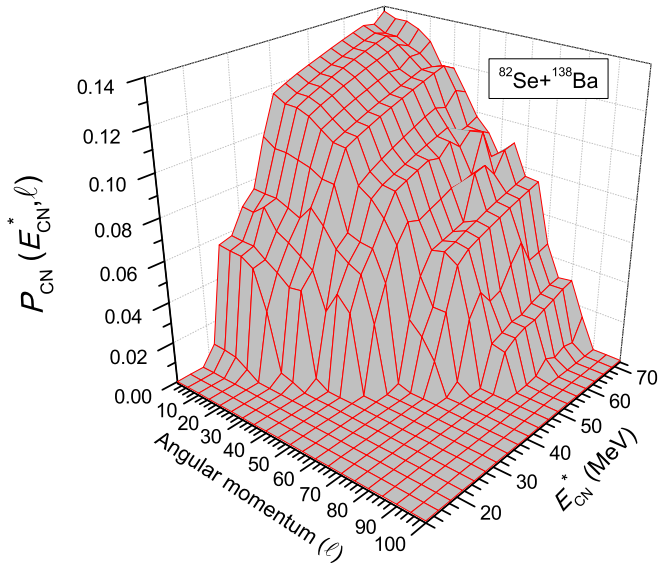

FIG. 11. (Color online) The fusion probability $P_{CN}(E^*_{CN},\ell) = \sigma_{fus}(E^*_{CN},\ell)/\sigma_{cap}(E^*_{CN},\ell)$ calculated for the ^{82}Se + ^{138}Ba reaction as a function of the CN excitation energy and angular momentum.

IV. COMPARISON OF THE EVAPORATION RESIDUE EXCITATION FUNCTIONS

Results of the partial cross sections of the CN formation are used to calculate evaporation residue cross sections at given values of the CN excitation energy E^*_{CN} and angular momentum ℓ by the advanced statistical model [22]

$$\sigma^x_{ER}(E^*_x) = \Sigma^{\ell_d}_{\ell=0}(2\ell+1)\sigma^x_{ER}(E^*_x,\ell), \tag{10}$$

where $\sigma^x_{ER}(E^*_x,\ell)$ is the partial cross section of ER formation obtained after the emission of particles $\nu(x)n + y(x)p + k(x)\alpha + s(x)$ [where $\nu(x)$, y, k, and s are numbers of neutrons, protons, α particles, and γ quanta] from the intermediate nucleus with excitation energy E^*_x at each step x of the de-excitation cascade by the formula (see Refs. [10,22,23])

$$\sigma^x_{ER}(E^*_x,\ell) = \sigma^x_{ER}(E^*_{x-1},\ell)W^x_{sur}(E^*_x,\ell). \tag{11}$$

In Eq. (11), $\sigma^x_{ER}(E^*_{x-1},\ell)$ is the partial cross section of the intermediate excited nucleus formation at the $(x-1)$th step, and W^x_{sur} is the survival probability of the xth intermediate nucleus against fission along the deexcitation cascade of CN; obviously

$$\sigma^{(0)}_{ER}(E^*_0,\ell) = \sigma_{fus}(E^*_{CN},\ell),$$

i.e., the first evaporation starts from the heated and rotating CN and $E^*_0 = E^*_{CN} = E_{c.m.} + Q_{gg} - V_{rot}(\ell)$; $V_{rot}(\ell)$ is the rotational energy of the CN.

The fission barrier decreases by the increase of the angular momentum ℓ and, therefore, in calculation of $W^{(x-1)}_{sur}(E^*_x,\ell)$ the fission barrier is used a sum of the parametrized macroscopic fission barrier $B^m_{fis}(\ell)$ depending on the angular momentum J [24] and the microscopic (shell) correction δW,

$$B_{fis}(\ell,T) = c\ B^m_{fis}(\ell) - h(T)\,q(\ell)\,\delta W, \tag{12}$$

where $c = 1$; $h(T)$ and $q(\ell)$ represent the damping functions of the nuclear shell correction δW by the increase of the excitation energy E_x and angular momentum ℓ, respectively [22]:

$$h(T) = \{1 + \exp[(T - T_0)/d]\}^{-1} \tag{13}$$

and

$$q(\ell) = \{1 + \exp[(\ell - \ell_{1/2})/\Delta\ell]\}^{-1}, \tag{14}$$

where, in Eq. (13), $T = \sqrt{E^*/a}$ represents the nuclear temperature depending on the excitation energy E^* and the level density parameter a, $d = 0.3$ MeV is the rate of washing out the shell corrections with the temperature, and $T_0 = 1.16$ MeV is the value at which the damping factor $h(T)$ is reduced by $1/2$; analogously, in Eq. (14), $\Delta\ell = 3\hbar$ is the rate of washing out the shell corrections with the angular momentum, and $\ell_{1/2} = 20\hbar$ is the value at which the damping factor $q(\ell)$ is reduced by $1/2$. Also, this procedure allows the shell corrections to become dynamical quantities. Therefore, if the capture process of the beam by the target takes place, the fission barrier disappears at $\ell > 40$ due to damping of the shell correction by $q(\ell)$.

Comparison of the results of ER cross sections for the four reactions under discussion allows us to reveal the role of the entrance channel properties in the formation of the reaction products. The theoretical methods applied in this work allow us to take into account the properties of the PES, and peculiarities of the angular momentum distribution of the DNS and CN formed in these reactions, which are very important in order to explain the difference among the corresponding ER results. In Fig. 12 the theoretical excitation functions of the xn evaporation residues formed after neutron emission only in the ^{16}O + ^{204}Pb (dashed line), ^{40}Ar + ^{180}Hf (dot-dashed line), ^{82}Se + ^{138}Ba (solid line) and ^{124}Sn + ^{96}Zr (dotted line) reactions are compared. As expected, the largest cross section of the evaporation residue's yield belongs to the more asymmetric ^{16}O + ^{204}Pb reaction since the fusion excitation function of this reaction is highest among the others

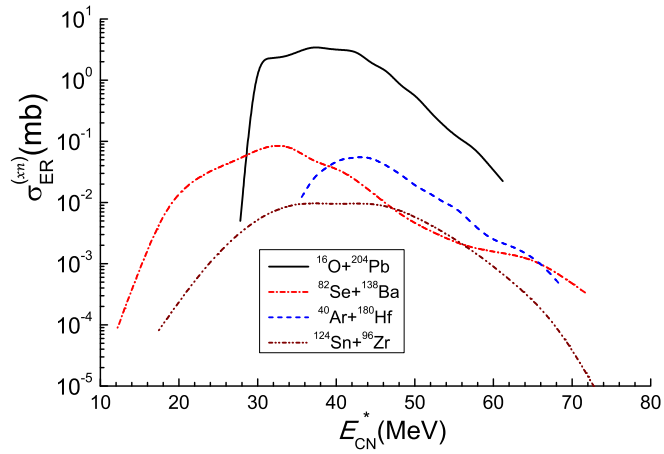

FIG. 12. (Color online) Comparison between the theoretical excitation functions of the evaporation residues formed after neutron emission only in the ^{16}O + ^{204}Pb (dashed line), ^{40}Ar + ^{180}Hf (dot-dashed line), ^{82}Se + ^{138}Ba (solid line), and ^{124}Sn + ^{96}Zr (dotted line) reactions.

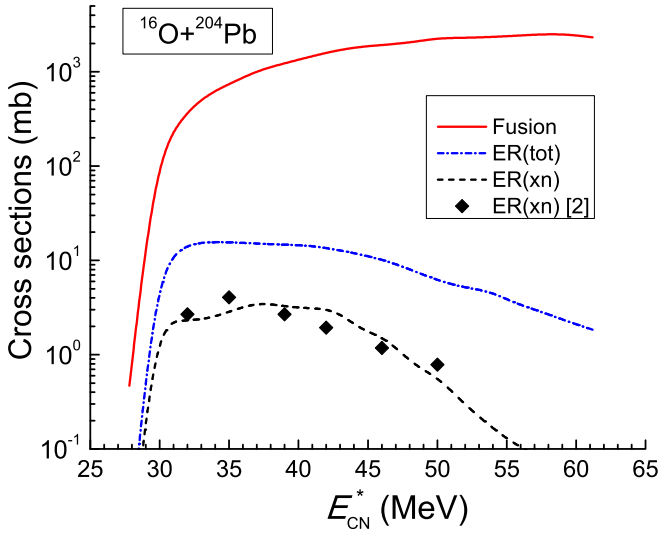

FIG. 13. (Color online) Comparison between the excitation functions of the total evaporation residues (dot-dashed line) and only neutron emission (dashed line) channels calculated for the ^{16}O + ^{204}Pb reaction with the experimental data (diamonds) [3] of the total neutron emission channels. The solid line shows the fusion excitation function calculated in this work.

(see Fig. 6). The evaporation residue cross sections are well reproduced by the use of the angular momentum distribution of the CN calculated in this work. The comparison of the theoretical excitation functions of the xn ER cross sections with the experimental data of the ^{16}O + ^{204}Pb reaction is presented in Fig. 13.

However, the excitation functions of the xn evaporation residues for the ^{40}Ar + ^{180}Hf reaction are about two orders of magnitude lower than the ones of the ^{16}O + ^{204}Pb reaction. The main reasons causing this difference are the relatively small capture cross section (see Fig. 5) and hindrance to complete fusion due to shell effect near ^{48}Ca (see Fig. 2).

During the evolution of the DNS formed in the ^{40}Ar + ^{180}Hf reaction, the charge and mass distributions of the system are shifted to the ^{48}Ca region. This behavior of the center of the charge distribution is seen in Fig. 14, which shows the evolution of the DNS charge distribution as a function of time. It is calculated by the method presented in Refs. [10,13]. As a result, the intrinsic fusion barrier B^*_{fus} becomes larger, causing the hindrance to complete fusion (see Fig. 10) since the driving potential has a minimum corresponding to the DNS fragment ^{48}Ca.

By increasing the beam energy, the ER cross section of the ^{40}Ar + ^{180}Hf reaction increases due to the increase of capture and fusion cross sections since the partial wave numbers contributing to the capture of colliding nuclei increase. But, the excitation function of the xn evaporation residues reaches a maximum value at $E^*_{CN} = 44$ MeV (see Fig. 12), and then it decreases by the increase of E^*_{CN} since in this range the number of deexcitation channels increases due to the contribution of the emission of charged particles (alpha particle and proton). The maximum value of the total ER cross sections for the ^{40}Ar + ^{180}Hf reaction is reached at $E^*_{CN} = 50$ MeV (see

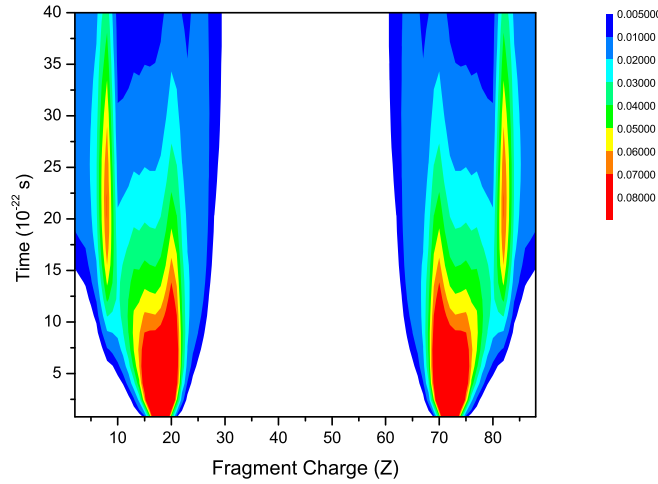

FIG. 14. (Color online) The charge distribution of the DNS fragments as a function of the interaction time for the ^{40}Ar + ^{180}Hf reaction.

Fig. 15), and then it decreases with the increase of E^*_{CN} despite the fusion cross section still increasing and saturating. Such a behavior of the total ER cross section versus E^*_{CN} is related to the decrease of the survival probabilities of the intermediate excited nuclei at higher excitation energies ($E^*_{CN} > 50$ MeV) due to the increase of fission products yield. The increase of the beam energy leads to the increase of the large values of ℓ which decreases the fission barrier at beam energies corresponding to the range $E^*_{CN} > 50$ MeV. Note that the ^{40}Ar + ^{180}Hf reaction is asymmetric and, due to the large size of the potential well of the nucleus-nucleus interaction, the large number of partial waves contributes to the formation of the CN (see Fig. 8).

The xn and total ER excitation function for the ^{82}Se + ^{138}Ba reaction are about one and two orders of magnitude, respectively, higher than the ones of the ^{124}Sn + ^{96}Zr reaction (see Figs. 12 and 15). Certainly, this is a result of the difference between the fusion excitation functions of these reactions (see Fig. 6). As one can see from this figure, the threshold excitation

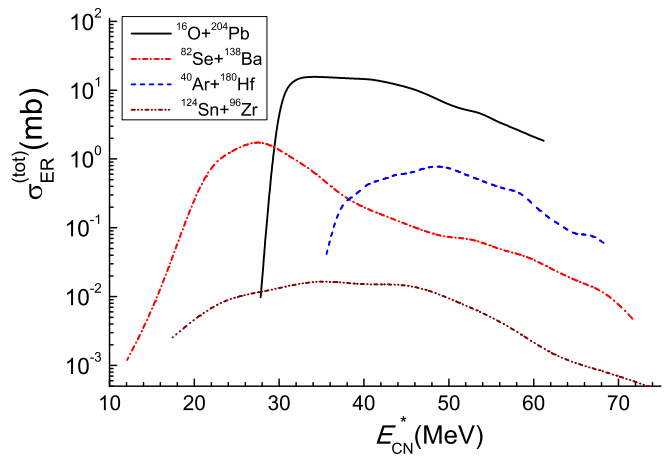

FIG. 15. (Color online) The same as in Fig. 12 but for the total evaporation residues.

energy of fusion for the ^{82}Se + ^{138}Ba reaction is lower than the one for the ^{124}Sn + ^{96}Zr reaction. The fusion excitation function of the former reaction grows much faster than one for the latter reaction. The slow increase of the fusion probability for the ^{124}Sn + ^{96}Zr reaction was extracted from the analysis of the measured evaporation residues cross sections by the authors of Ref. [2]. In our calculations we use the shape parameters corresponding to the lowest-lying 2^+ and 3^- states of projectile and target (see Table I in Appendix A).

The prevalence of the ER yield cross section of the ^{82}Se + ^{138}Ba reaction at excitation energies $E^*_{CN} < 38$ MeV over the one in the ^{40}Ar + ^{180}Hf reaction is seen from Figs. 12 and 15. An interesting observation is that the maximum value of the ER excitation function of the ^{82}Se + ^{138}Ba reaction is substantially larger than the one of the ^{40}Ar + ^{180}Hf reaction. It is well known that the low excitation energy E^*_{CN} is favorable for the survival probability of the heated CN against fission. But in the case of the asymmetric ^{40}Ar + ^{180}Hf reaction the excitation energy range $E^*_{CN} < E^*_{thr} = 35$ MeV is not reachable since the energy balance $Q_{gg} = -99.49$ MeV value is small. Therefore, at beam energies $E_{c.m.} < E^*_{thr} - Q_{gg}$ the capture events do not occur while for the ^{82}Se + ^{138}Ba reaction the energy balance is $Q_{gg} = -180.52$ MeV, which allows for the CN to be formed with an excitation energy about 12–14 MeV. This is connected with the shell effects in colliding nuclei: ^{138}Ba has 82 (magic number) neutrons. At beam energies corresponding to the range $E^*_{CN} > 38$ MeV the fusion cross section of the ^{40}Ar + ^{180}Hf reaction increases sharply, causing the strong increase of the ER cross sections, which become higher than the ones of the ^{82}Se + ^{138}Ba reaction. The different trends of dependence of the ER cross sections (see Fig. 15) for these two reactions in the $E^*_{CN} = 40-50$ MeV range are explained by the difference between the numbers of the partial waves contributing to the CN formation in Eq. (5) and by the decrease of the survival probabilities with increasing CN angular momentum (see Fig. 16).

Figure 16 shows the survival probability as a function of the CN angular momentum and excitation energy for the ^{82}Se + ^{138}Ba reaction. It is clearly seen that the survival probability reaches maximum values at low excitation energies, $E^*_{CN} =$ 21–23 MeV, where the total ER cross section is very large since the range of the angular momentum is wide enough, $\ell =$ 0–35. As E^*_{CN} increases from 20 to 70 MeV, the range of the angular momentum contributing to the total ER cross section is reduced two times: mainly the range $\ell =$ 0–18 contributes to the results. Therefore, the total ER cross section strongly decreases in the range $E^*_{CN} =$ 30–70 MeV though the fusion cross section is approximately saturated (see the dot-dashed line in Fig. 6). This result shows the importance of taking into account of the dependence of the survival probability on the angular momentum and excitation energy of a fissioning nucleus. The contribution of the angular momentum range $\ell =$ 19–35 to the total ER yields is very small since the fission barrier decreases with the increase of ℓ.

Nevertheless, the total ER cross sections for the mass asymmetric ^{40}Ar + ^{180}Hf reaction are larger than the ones of the ^{82}Se + ^{138}Ba reaction at larger excitation energies $E^*_{CN} > 38$ MeV. This is related to the large probability of CN formation at large values of angular momentum which

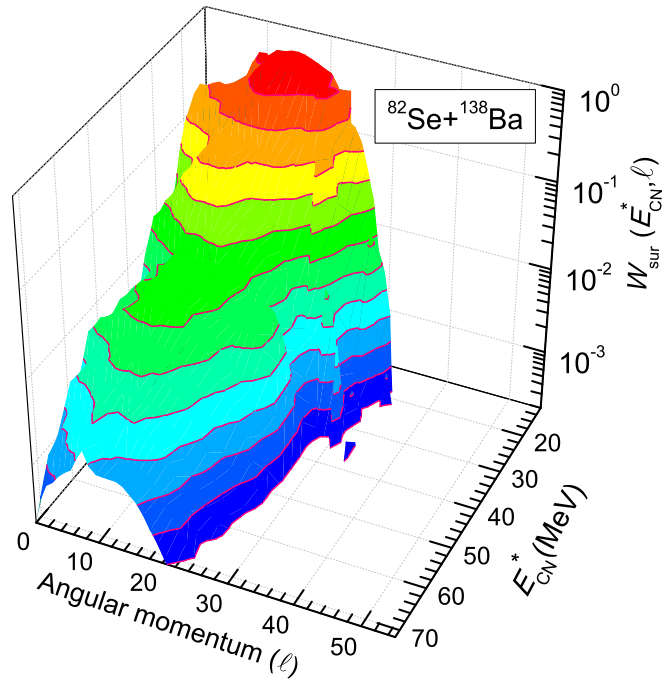

FIG. 16. (Color online) The survival probability $W_{sur}(E^*_{CN},\ell)$ calculated for the ^{82}Se + ^{138}Ba reaction as a function of the CN excitation energy and angular momentum.

can be seen in Fig. 8. Although this figure is for the partial capture cross section, the partial fusion cross section is similar due to the large value of the fusion probability P_{CN} for the ^{40}Ar + ^{180}Hf reaction. The presence of the contribution of large values of $L = \ell\hbar$ is confirmed by the experimental data of this reaction. The larger values of the total ER cross sections measured in the experiment [25] indicate the larger contribution of the alpha particle emission by the CN during its deexcitation in the $E^*_{CN} > 38$ MeV range. The difference among the xn ER cross sections of these reactions is not so large since neutron emission is not sensitive to the value of angular momentum.

The individual channels of neutron emission for the ^{40}Ar + ^{180}Hf, ^{82}Se + ^{138}Ba, and ^{124}Sn + ^{96}Zr reactions are presented in Figs. 17, 18, and 19, respectively. Peculiarities of the excitation functions of the individual deexcitation channels allow us to have information about properties of the processes during the formation of the CN in these reactions. The $4n$ ER cross section is dominant in the ^{40}Ar + ^{180}Hf reaction while the $3n$ ER channel is dominant in the ^{82}Se + ^{138}Ba reaction. These ER channels are nearly comparable in the ^{124}Sn + ^{96}Zr reaction. The threshold value of the excitation energy to complete fusion for the ^{40}Ar + ^{180}Hf reaction is $E^*_{thr} = 35$ MeV and, therefore, the lower energetic part of the $3n$ ER channel is suppressed. The fusion threshold value of E^*_{CN} of the ^{82}Se + ^{138}Ba reaction is about 14 MeV due to the large Q_{gg} value. Therefore, there is a favorable condition for realization of the $3n$ ER channel in this reaction. The results of this work show the possibility to observe the $2n$ ER channel (thin solid curve in Fig. 18) in the ^{82}Se + ^{138}Ba reaction.

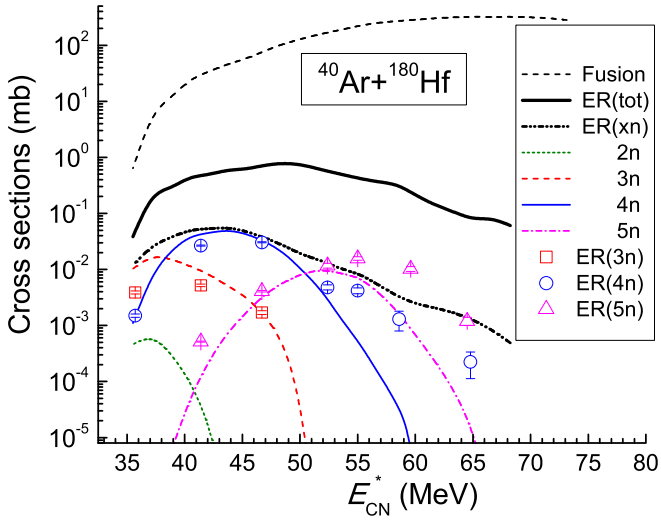

FIG. 17. (Color online) Comparison between the excitation functions of $2n$ (dotted line), $3n$ (thin dashed line), $4n$ (thin solid line), and $5n$ (thin dot-dashed line) ER channels calculated in this work for the ^{40}Ar + ^{180}Hf reaction with the ones measured in the experiment [25] for the $3n$ (squares), $4n$ (circles), and $5n$ (triangles) ER channels. The excitation functions of the total evaporation residues (thick solid line) and of only the neutron emission (thick dot-dashed line) channels, as well as of complete fusion (thick dashed line) calculated in this work are presented.

The hindrance to complete fusion is manifested clearly in the case of the more symmetric ^{124}Sn + ^{96}Zr reaction. The threshold value E^*_{CN} is about 17 MeV for this reaction, but the complete fusion excitation function increases slowly with

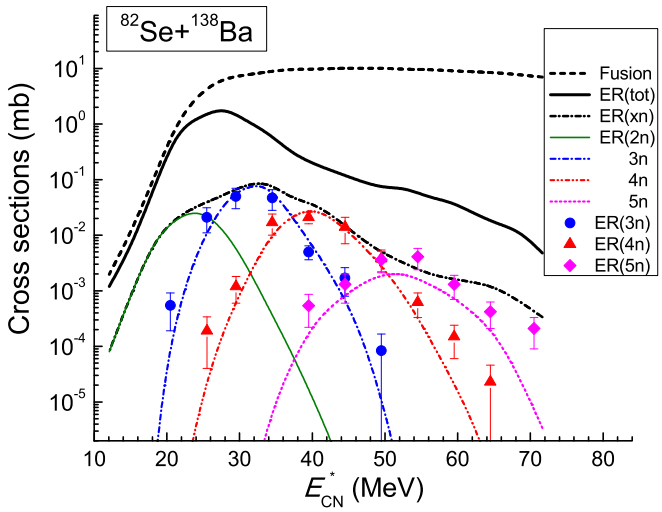

FIG. 18. (Color online) Comparison between the excitation functions of $2n$ (thin solid line), $3n$ (thin dot-dashed line), $4n$ (thin dot-dot-dashed line), and $5n$ (thin dotted line) ER channels calculated in this work for the ^{82}Se + ^{138}Ba reaction with the ones measured in the experiment [26] for the $3n$ (circles), $4n$ (triangles), and $5n$ (diamonds) ER channels. The excitation functions of the total evaporation residues (thick solid line) and of only the neutron emission (thick dot-dashed line) channels, as well as of complete fusion (thick dashed line) calculated in this work are presented.

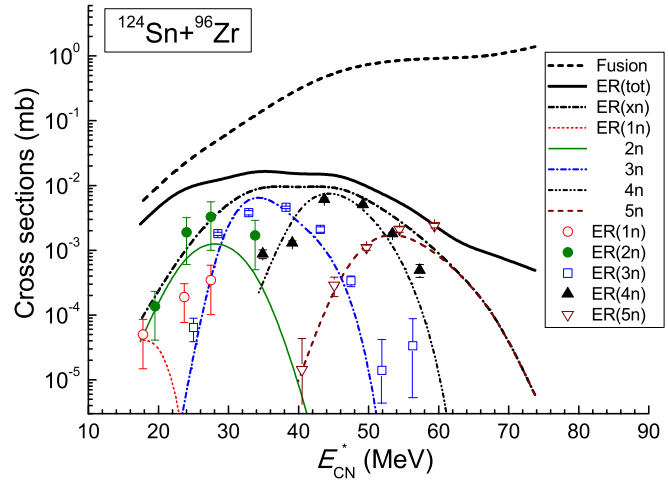

FIG. 19. (Color online) Comparison between the excitation functions of $1n$ (thin dotted line), $2n$ (solid line), $3n$ (thin dot-dashed line), $4n$ (thin dot-dot-dashed line), and $5n$ (thin dashed line) ER channels calculated in this work for the ^{124}Sn + ^{96}Zr reaction with the ones measured in the experiment [2] for the $1n$ (open circles), $2n$ (filled circles), $3n$ (open squares), $4n$ (filled triangles), and $5n$ (open triangles) ER channels. The excitation functions of the total evaporation residues (thick solid line) and of only the neutron emission (thick dot-dashed line) channels, as well as of complete fusion (thick dashed line) calculated in this work are presented.

increasing beam energies (dot-dot-dashed curve in Fig. 6). Therefore, though the $2n$ and $3n$ ER channels are open, their ER cross sections are not dominant. We have a not-so-large difference in the maximum values of the $2n$, $3n$, and $4n$ ER cross sections for the ^{124}Sn + ^{96}Zr reaction. The $1n$ and $5n$ ER cross sections are smaller since the $1n$ channel is suppressed due to fusion hindrance and the $5n$ channel has very strong competition with the fission channel at large values of E^*_{CN}.

To analyze the effect of the angular momentum distribution for the CN formed in different reactions we compare the partial fusion cross sections of the ^{82}Se + ^{138}Ba and ^{124}Sn + ^{96}Zr reactions in Figs. 20 and 21, respectively. It is seen that the main

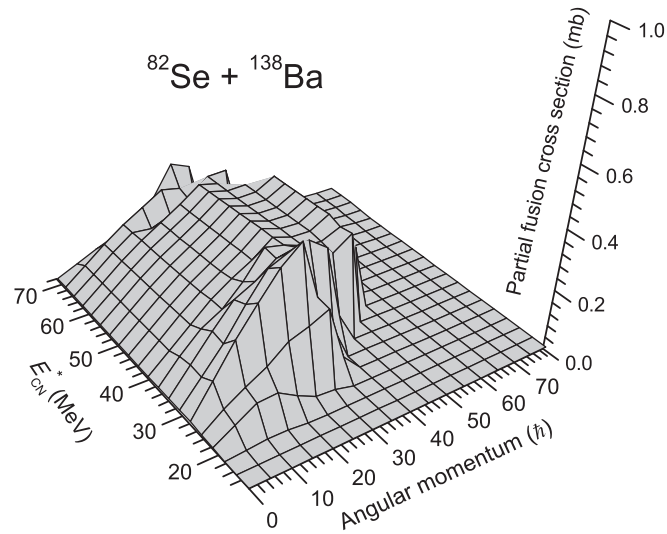

FIG. 20. Partial fusion cross section of the ^{82}Se + ^{138}Ba reaction.

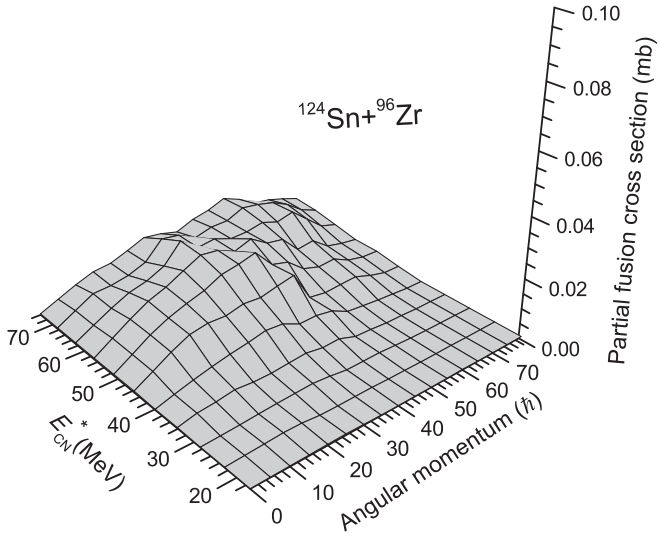

FIG. 21. Partial fusion cross section of the ^{124}Sn + ^{96}Zr reaction.

contribution is from the angular momentum in the range $0 < L < 50\hbar$ for the CN formed in the ^{82}Se + ^{138}Ba reaction (see Fig. 20) while this range is extended up to values $L = 70\hbar$ in the case of the ^{124}Sn + ^{96}Zr reaction (see Fig. 21). The partial fusion cross sections of the reaction with ^{82}Se are much larger than the ones for the reaction with ^{124}Sn. Note that the partial fusion cross section axes of Figs. 20 and 21 have different scales. As we discussed above (see Fig. 16), the contribution of the large values of L to the ER cross sections is small due to the strong dependence of the fission barrier on the angular momentum [22,24]. Therefore, the ER cross sections of all these reactions analyzed in this work decrease at high values of E^*_{CN} corresponding to beam energies sufficiently higher than the Coulomb barrier where the fusion cross section increases or saturates (see Figs. 13, 17, 18, and 19). The partial fusion cross sections of the ^{124}Sn + ^{96}Zr reaction are smaller in comparison with the other reactions even at small values of E^*_{CN}.

V. CONCLUSIONS

To study the entrance channel effects on the ER yields in reactions leading to the same CN we compared the capture, fusion, and ER cross sections calculated by the use of the combined dinuclear system and advanced statistical models. The difference between evaporation residue cross sections can be related to the stage of formation of the CN or its surviving stage against fission by emission of neutrons and charged particles.

The comparison showed that the capture excitation functions obtained for the mass asymmetric ^{16}O + ^{204}Pb and ^{40}Ar + ^{180}Hf reactions are one order of magnitude higher than the ones for the almost symmetric ^{82}Se + ^{138}Ba and ^{124}Sn + ^{96}Zr reactions. The stronger Coulomb force makes the potential well shallower, and as a result the decrease of the number of partial waves $[\ell_d(E)]$ causes decreasing capture cross section.

The fusion excitation functions of the ^{82}Se + ^{138}Ba and ^{124}Sn + ^{96}Zr reactions are even two orders of magnitude lower than the ones of the mass asymmetric reactions. This result is explained by the hindrance to complete fusion due to the larger intrinsic fusion barrier B^*_{fus} for the transformation of the DNS into the CN and the smaller quasifission barrier B_{qf} in comparison with values of the corresponding quantities for the more asymmetric reactions. According to our calculations B^*_{fus} increases and B_{qf} decreases with the decrease of the mass asymmetry reactions.

Results of the partial cross sections of the CN formation are used to calculate evaporation residue cross sections at given values of the CN excitation energy E^*_{CN} and angular momentum ℓ by the advanced statistical model. The comparison of the theoretical excitation functions of the xn evaporation residues formed in the ^{16}O + ^{204}Pb, ^{40}Ar + ^{180}Hf, ^{82}Se + ^{138}Ba, and ^{124}Sn + ^{96}Zr reactions shows that the evaporation residue yields of the ^{16}O + ^{204}Pb reaction are larger than the ones of the other three reactions since the fusion excitation function of this reaction is the highest. There is no hindrance to complete fusion.

The xn and total ER excitation functions for the almost symmetric ^{82}Se + ^{138}Ba reaction are about one and two orders of magnitude, respectively, higher than the ones of another similar ^{124}Sn + ^{96}Zr reaction. This is explained by the fact that the fusion excitation function of the former reaction is higher than the one of the latter reaction.

The unusual prevalence of the ^{82}Se + ^{138}Ba reaction for the ER yields in the range $E^*_{CN} < 38$ MeV in comparison with the mass asymmetric ^{40}Ar + ^{180}Hf reaction, which has a larger fusion excitation function at $E^*_{CN} > 38$ MeV, is analyzed. The maximum value of the ER excitation function of the ^{82}Se + ^{138}Ba reaction is sufficiently larger than the one of the ^{40}Ar + ^{180}Hf reaction. The large values of the ER excitation function of the ^{82}Se + ^{138}Ba reaction are observed in the $E^*_{CN} < 35$ MeV energy range where the fusion in the reaction induced by ^{40}Ar is strongly hindered by the Coulomb barrier of the entrance channel. Therefore, due to relatively small Q_{gg} value (−99.49 MeV) for the reaction with ^{40}Ar, the lowest value of the excitation energy is $E^*_{CN} = 35$ MeV. Nevertheless, for the $E^*_{CN} > 38$ MeV energy range the total ER yields produced by the ^{40}Ar + ^{180}Hf reaction are higher than the ones produced by the ^{82}Se induced reaction due to the strong increase of the fusion cross section of the former reaction.

The decrease of the total ER yields with the increase of the E^*_{CN} energy is revealed as a trend for all reactions, since the survival probability W_{sur} decreases with the increase of the fission probability.

At large beam energies the number of partial waves contributing to fusion increases, causing the decrease of the fission barrier [24]. The presence of the contribution of large values of L is confirmed by the larger values of the total ER cross sections measured in the experiment [25]. The larger values of the total ER cross sections indicate the large contribution of the charged (proton and alpha) particles emission by the CN during its deexcitation in the $E^*_{CN} > 38$ MeV range. The difference between the xn ER cross sections of these reactions is not so much since neutron emission is not sensitive to the value of angular momentum.

The comparison of the ER cross sections calculated for the ^{40}Ar + ^{180}Hf and ^{82}Se + ^{138}Ba reactions shows that the fusion probability P_{CN} and the survival probability W_{sur} are important quantities characterizing different stages of the reaction during the formation of the CN and its survival against fission.

The theoretical analysis of the measured data of the yield of the xn, total, and individual ER by the combined DNS and advanced statistical models allows us to reveal the important role of the angular momentum distribution of capture, complete fusion, and deexcitation stages of the mass asymmetric and mass symmetric reactions.

ACKNOWLEDGMENTS

This work was supported by the Rare Isotope Science Project of Institute for Basic Science funded by the Ministry of Science, ICT and Future Planning (MSIP) and the National Research Foundation of Korea (2013M7A1A1075766). A.K.N. is grateful to Prof. Yongseok Oh for the fruitful discussion of the results and Department of Physics of the Kyungpook National University for the warm hospitality during his staying by the support of the Brain Pool Program No. 142S-1-3-1034 of the MSIP. A.K.N. thanks Russian Foundation for Basic Research for the partial support in the performance of this work.

APPENDIX A: DEFORMED NUCLEI

The expectation values of the capture and fusion cross sections are obtained by averaging the contributions of collisions with different values of the orientation angle, α, which is the angle of the nucleus relatively to the beam direction at the initial stage of reaction:

$$\langle \sigma_i(E_{\text{c.m.}}) \rangle = \int_0^{\pi/2} \sin\alpha \, \sigma_i(E_{\text{c.m.}};\alpha) d\alpha. \quad \text{(A1)}$$

Deformation parameters (see Table I) of the ground quadrupole and octupole states are taken from Ref. [17] of the reacting nuclei in this work while the ones of the first excited first 2^+ and 3^- states are obtained from Refs. [27] and [28], respectively.

TABLE I. Deformation parameters of the ground state and the first excited 2^+ and 3^- states used in the calculations in this work.

Nucleus	β_2	β_3	β_{2+} [27]	β_{3-} [28]
^{16}O	0.021	0.0	0.364	0.37
^{204}Pb	−0.008	0.0	0.41	0.114
^{40}Ar	0.0	0.0	0.284	0.26
^{180}Hf	0.279	0.0	0.274	0.07
^{82}Se	0.154	0.0	0.193	0.161
^{138}Ba	0.0	0.0	0.093	0.118
^{124}Sn	0.0	0.0	0.095	0.27
^{96}Zr	0.217	0.0	0.080	0.133

APPENDIX B: SURFACE VIBRATION

If a nucleus has spherical shape in its ground state and its first 2^+ excited state is deformed, this excited state was considered as the vibrational state. The surface vibrations are regarded as independent harmonic vibrations and the nuclear radius is considered to be distributed as a Gaussian distribution [29],

$$g(\beta_2,\beta_3) = \exp\left[-\frac{[\sum_\lambda \beta_\lambda Y^*_{\lambda 0}(\alpha)]^2}{2\sigma_\beta^2} \right] \left(2\pi\sigma_\beta^2\right)^{-1/2}, \quad \text{(B1)}$$

where α is the direction of the spherical nucleus. For simplicity, we use $\alpha = 0$.

$$\sigma_\beta^2 = R_0^2 \sum_\lambda \frac{2\lambda+1}{4\pi} \frac{\hbar}{2D_\lambda \omega_\lambda} = \frac{R_0^2}{4\pi} \sum_\lambda \beta_\lambda^2, \quad \text{(B2)}$$

$$\langle \sigma_i(E_{\text{c.m.}}) \rangle = \int_{-\beta_{2+}}^{\beta_{2+}} \int_{-\beta_{3-}}^{\beta_{3-}} \sigma_i(E_{\text{c.m.}}) g(\beta_2,\beta_3) d\beta_2 d\beta_3 \quad \text{(B3)}$$

[1] B. B. Back, H. Esbensen, and C. L. Liang, Rev. Mod. Phys. **86**, 317 (2014).
[2] C. C. Sahm, H.-G. Clerc, K.-H. Schmidt, W. Reisdorf, P. Armbruster, F. P. Heßberger, J. G. Keller, G. Münzenberg, and D. Vermeulen, Z. Phys. A **319**, 113 (1984).
[3] D. J. Hinde, M. Dasgupta, and A. Mukherjee, Phys. Rev. Lett. **89**, 282701 (2002).
[4] A. Yu. Chizhov, M. G. Itkis, I. M. Itkis, G. N. Kniajeva, E. M. Kozulin, N. A. Kondratiev, I. V. Pokrovsky, R. N. Sagaidak, V. M. Voskressensky, A. V. Yeremin, L. Corradi, A. Gadea, A. Latina, A. M. Stefanini, S. Szilner, M. Trotta, A. M. Vinodkumar, S. Beghini, G. Montagnoli, F. Scarlassara, A. Ya. Rusanov, F. Hanappe, O. Dorvaux, N. Rowley, and L. Stuttgé, Phys. Rev. C **67**, 011603(R) (2003).
[5] G. Fazio, G. Giardina, A. Lamberto, R. Ruggeri, C. Sacca, R. Palamara, A. I. Muminov, A. K. Nasirov, U. T. Yakhshiev, F. Hanappe, T. Materna, and L. Stuttge, J. Phys. Soc. Jpn. **72**, 2509 (2003).
[6] M. Dasgupta and D. J. Hinde, Nucl. Phys. A **734**, 148 (2004).
[7] G. Fazio, G. Giardina, G. Mandaglio, R. Ruggeri, A. I. Muminov, A. K. Nasirov, Yu. Ts. Oganessian, A. G. Popeko, R. N. Sagaidak, A. V. Yeremin, S. Hofmann, F. Hanappe, and C. Stodel, Phys. Rev. C **72**, 064614 (2005).
[8] G. Adamian, N. Antonenko, and W. Scheid, in *Clusters in Nuclei*, edited by C. Beck, Lecture Notes in Physics No. 848 (Springer, Heidelberg, 2012), Vol. 2, p. 165.
[9] G. Fazio, G. Giardina, A. Lamberto, C. Saccà, R. Palamara, A. I. Muminov, A. K. Nasirov, K. V. Pavliy, F. Hanappe, T. Materna, and L. Stuttgé, J. Phys. Soc. Jpn. **74**, 307 (2005).
[10] A. Nasirov, A. Fukushima, Y. Toyoshima, Y. Aritomo, A. Muminov, S. Kalandarov, and R. Utamuratov, Nucl. Phys. A **759**, 342 (2005).
[11] G. Fazio, G. Giardina, F. Hanappe, G. Mandaglio, M. Manganaro, A. I. Muminov, A. K. Nasirov, and C. Sacca, J. Phys. Soc. Jpn. **77**, 124201 (2008).
[12] G. Mandaglio, G. Fazio, G. Giardina, F. Hanappe, M. Manganaro, A. I. Muminov, A. K. Nasirov, and C. Saccá, Phys. At. Nucl. **72**, 1639 (2009).

[13] G. Fazio, G. Giardina, G. Mandaglio, F. Hanappe, A. I. Muminov, A. K. Nasirov, W. Scheid, and L. Stuttge, Mod. Phys. Lett. A **20**, 391 (2005).
[14] B. B. Back, R. R. Betts, J. E. Gindler, B. D. Wilkins, S. Saini, M. B. Tsang, C. K. Gelbke, W. G. Lynch, M. A. McMahan, and P. A. Baisden, Phys. Rev. C **32**, 195 (1985).
[15] A. K. Nasirov, G. Mandaglio, M. Manganaro, A. I. Muminov, G. Fazio, and G. Giardina, Phys. Lett. B **686**, 72 (2010).
[16] G. Audi and A. H. Wapstra, Nucl. Phys. A **595**, 409 (1995).
[17] P. Möller, J. R. Nix, W. D. Myers, and W. J. Swiatecki, At. Data Nucl. Data Tables **59**, 185 (1995).
[18] N. V. Antonenko, E. A. Cherepanov, A. K. Nasirov, V. P. Permjakov, and V. V. Volkov, Phys. Lett. B **319**, 425 (1993); Phys. Rev. C **51**, 2635 (1995).
[19] Fazio, G. Giardina, A. Lamberto, A. I. Muminov, A. K. Nasirov, F. Hanappe, and L. Stuttge, Eur. Phys. J. A **22**, 75 (2004).
[20] P. Fröbrich and R. Lipperheide, *Theory of Nuclear Reactions* (Clarendon Press, Oxford, 1996).
[21] A. K. Nasirov, G. Giardina, G. Mandaglio, M. Manganaro, F. Hanappe, S. Heinz, S. Hofmann, A. I. Muminov, and W. Scheid, Phys. Rev. C **79**, 024606 (2009).
[22] G. Mandaglio, G. Giardina, A. K. Nasirov, and A. Sobiczewski, Phys. Rev. C **86**, 064607 (2012).
[23] G. Giardina, S. Hofmann, A. I. Muminov, and A. K. Nasirov, Eur. Phys. J. A **8**, 205 (2000).
[24] A. J. Sierk, Phys. Rev. C **33**, 2039 (1986).
[25] D. Vermeulen, H.-G. Clerc, and C. C. Sahm, Z. Phys. A **318**, 157 (1984).
[26] K. Satou, H. Ikezoe, S. Mitsuoka, K. Nishio, and S. C. Jeong, Phys. Rev. C **65**, 054602 (2002).
[27] S. Raman, C. W. Nestor, Jr., and P. Tikkanen, At. Data Nucl. Data Tables **78**, 1 (2001).
[28] R. H. Spear, At. Data Nucl. Data Tables **42**, 55 (1989).
[29] H. Esbensen, Nucl. Phys. A **352**, 147 (1981).